

## Heavy ion double folding cluster optical potentials

M. El-Azab Farid

Physics Department, Assiut University, Assiut 71516, Egypt

(Received 11 December 2001; published 4 June 2002)

The  $\alpha$ -cluster model is used to construct the double folding cluster optical model potential of heavy ions interaction. The derived potential is employed to analyze elastic scattering data of  $^{32}\text{S}+^{24}\text{Mg}$  at 65, 75, 86, 95, and 110 MeV laboratory energies. An energy-dependent renormalization coefficient is necessary in order to obtain successful reproductions of the data.

DOI: 10.1103/PhysRevC.65.067303

PACS number(s): 21.60.Gx, 24.10.Ht, 25.70.Bc, 27.20.+n

It is well known that phenomenological optical potentials are often successfully used to describe the heavy ion (HI) elastic scattering data. The use of folding model (FM), however, is appealing because it allows one to predict the potentials of systems for which scattering data are not available. Furthermore, the folding potentials make it possible to eliminate ambiguities, which appear with the phenomenological ones.

In the last two decades or so, the FM for the real part of the optical potential has proved to give a good description of HI elastic and inelastic scattering data [1–4]. At the same time, the cluster model using the double folding (DF) potential has revealed to be quite successful for the comprehensive understanding of the structure of light and medium nuclei [5–9].

Recently, we used the alpha ( $\alpha$ )-cluster structure of light HI to generate the  $\alpha$ -nucleus and nucleus-nucleus single folding cluster [8] and double folding cluster (DFC) [9] potentials, respectively, based upon an  $\alpha$ - $\alpha$  interaction folded with the  $\alpha$ -particle distributions in the colliding nuclei. The derived potentials were successfully used to describe 27 sets of  $\alpha$  particles [8] and 20 sets of  $^{12}\text{C}$  and  $^{16}\text{O}$  [9] elastic scattering data from  $^{12}\text{C}$ ,  $^{16}\text{O}$ , and  $^{28}\text{Si}$  targets at a wide range of energies.

In the present work and another recent paper [10] we extend the DFC approach to construct optical potentials for medium HI systems. The present study is confined to analyze the  $^{32}\text{S}+^{24}\text{Mg}$  elastic scattering data at near- and sub-barrier

energies (65, 75, 86, 95, and 110 MeV) using the derived DFC potential. These data were recently [11] measured and analyzed using a DF potential based upon the M3Y nucleon-nucleon ( $NN$ ) interaction.

The DFC potential is defined as [9]

$$V_{DFC}(R) = \int \rho_1(r_1)\rho_2(r_2)V_{\alpha\alpha}(|\vec{R}-\vec{r}_1+\vec{r}_2|)d\vec{r}_1d\vec{r}_2, \quad (1)$$

where  $\rho_1$  and  $\rho_2$  are the density distributions of  $\alpha$  particles inside  $^{32}\text{S}$  and  $^{24}\text{Mg}$  nuclei, respectively, and  $V_{\alpha\alpha}$  is the interaction potential between an  $\alpha$  particle in the projectile ( $^{32}\text{S}$ ) and another  $\alpha$ -particle in the target ( $^{24}\text{Mg}$ ). The same treatment and form of interaction introduced in our previous studies [8,9] are used in the present calculations. The nuclear

TABLE I. Best fit parameters obtained from the analysis of  $^{32}\text{S}+^{24}\text{Mg}$  elastic scattering.

$E$ (MeV)	$N$	$W_0$ (MeV)	$r_I$ (fm)	$a_I$ (fm)	$J_I$ (MeV fm <sup>3</sup> )	$\sigma_R$ (mb)	$\chi^2$	
65	A	0.92	60.0	1.279	0.219	154	37.5	0.12
	B	0.89	6.46	1.394	0.230	21.4	47.1	0.14
75	A	0.84	52.6	1.305	0.376	145	429	0.24
	B	0.81	3.18	1.513	0.227	13.5	404	0.33
86	A	0.72	52.5	1.211	0.476	118	732	1.3
	B	0.71	19.7	1.294	0.464	53.5	726	1.3
95	A	0.65	60.0	1.139	0.586	115	974	1.74
	B	0.63	11.8	1.323	0.557	34.8	983	1.54
110	A	0.62	60.0	1.075	0.676	100	1257	5.4
	B	0.60	21.6	1.209	0.615	49.4	1200	2.77

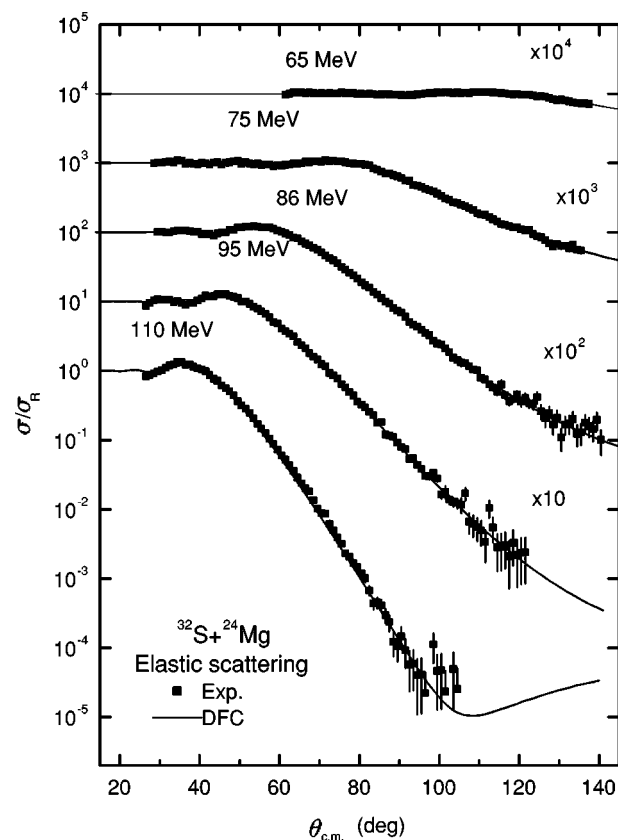


FIG. 1. Angular distributions of elastic scattering cross section for  $^{32}\text{S}+^{24}\text{Mg}$  reaction in comparison with DFC predictions.

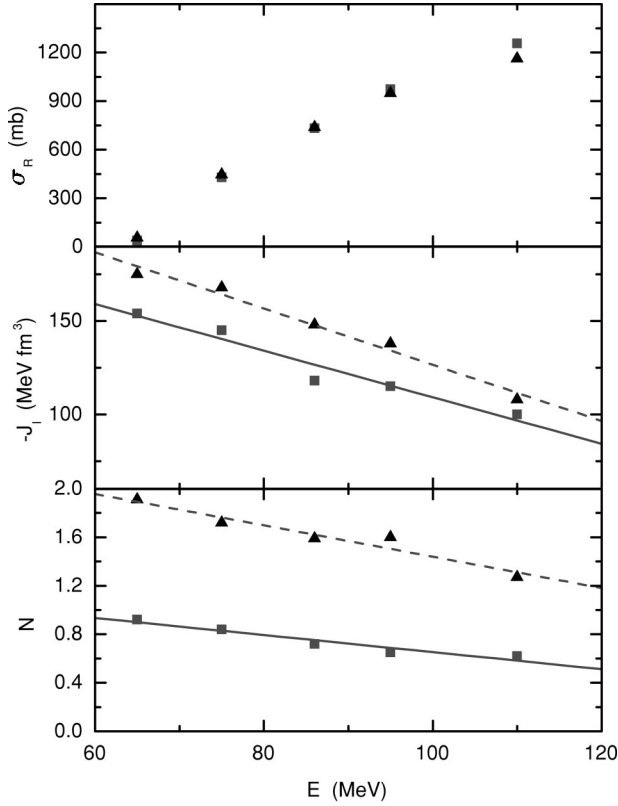


FIG. 2. Energy dependence of the renormalization coefficient  $N$  (lower part), volume integral of the imaginary part  $J_I$  (middle part), and total reaction cross section  $\sigma_R$  (upper part). Straight lines are the least-square fits. Squares for the present work and up triangles for Ref. [11].

density parameters of  $^{32}\text{S}$  and  $^{24}\text{Mg}$  nuclei required for the present calculations are taken from Ref. [12].

Then, the nucleus-nucleus interaction is considered as

$$U(R) = -NV_{DFC}(R) - iW(R) + V_C(R), \quad (2)$$

where  $N$  is a renormalization coefficient,  $W$  represents the imaginary part of the optical potential defined in a phenomenological Woods-Saxon (WS) radial form factor [13] and  $V_C$  is the Coulomb repulsive interaction with a radius  $R_C = 1.1(32^{1/3} + 24^{1/3})$  fm.

The computer code HIOPTIM94 [14] was used to calculate the angular distribution of the elastic scattering differential cross sections. Four free parameters were optimized;  $N$  and the imaginary WS parameters; the depth  $W_0$ , radius  $r_I$  and diffuseness  $a_I$ , in order to fit the data by minimizing the  $\chi^2$  parameter.

We start our analysis by fitting the elastic scattering data using the WS parameters obtained for the M3Y DF potential given in Table I of Ref. [11]. The present best fit parameters are shown in Table I as the set *A*. Then we used parameters of a shallow WS potential, which yielded the set *B*. Both sets produce almost identical predictions and comparable values for the  $\chi^2$  parameter and total reaction cross sections  $\sigma_R$ .

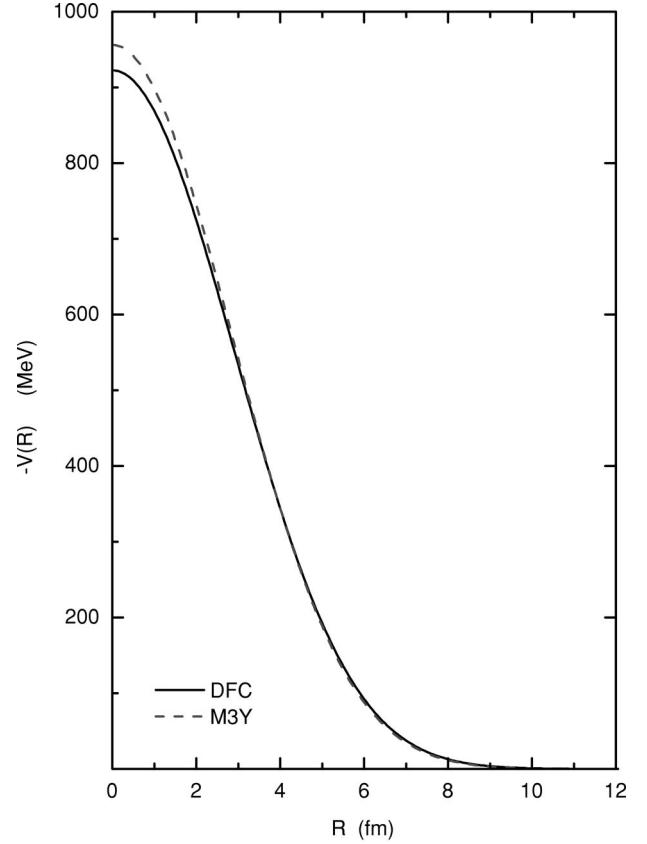


FIG. 3. A comparison between unnormalized DFC and M3Y potentials using the same nuclear matter densities of  $^{32}\text{S}$  and  $^{24}\text{Mg}$  nuclei.

Figure 1 demonstrates a comparison between experimental data and the predicted elastic scattering cross sections using set *A*.

As shown in Fig. 1, the renormalized real DFC potential successfully reproduces the data of all considered energies. We notice that the success of the derived DFC potential to predict the data is more pronounced at backward angles (larger than the rainbow angles) for the two highest energies than that found by the M3Y DF potential [11].

From Table I it is evident that the renormalization factor  $N$  has a clear energy dependence, where  $N$  decreases as energy increases. This result is consistent with that noticed for the renormalization of the M3Y DF potential [11] obtained from the analysis of the same data. In the lower part of Fig. 2 values for  $N$  are plotted against the energy  $E$  in comparison with the result of the previous analysis. Both results, as shown in the figure, have a linear energy dependence with the same energy dependence factor  $\sim (1 - 0.005E)$ , i.e., they have similar behaviors. The M3Y potential values, however, are larger than those of the DFC one by approximately a factor of 2. This behavior resembles that observed from the analysis of HI elastic scattering using the DFC potential based upon an  $\alpha$ -nucleon interaction and M3Y DF potential [9], which indicates that the DF model using the  $\alpha$ -cluster model yields successful DF potentials to reproduce HI elastic scattering.

On the other hand, it may be useful to compare the M3Y

potential with the DFC one. The M3Y DF potential is defined as

$$V_{M3Y}(R) = \int \rho_1(r_1) \rho_2(r_2) v_{nn}(|\vec{R} - \vec{r}_1 + \vec{r}_2|) d\vec{r}_1 d\vec{r}_2, \quad (3)$$

where  $\rho_1$  and  $\rho_2$  are the nuclear matter density distributions of  $^{32}\text{S}$  and  $^{24}\text{Mg}$  nuclei, respectively, and  $v_{nn}$  is the M3Y effective  $NN$  interaction used in Ref. [11], which is defined as

$$v_{nn}(s) = 7999 \frac{\exp(4s)}{4s} - 2134 \frac{\exp(2.5s)}{2.5s} - 262\delta(s), \quad (4)$$

where the  $\delta(s)$  term accounts for the knock-on exchange term. Usually, this term is used in the case of weak energy dependence. However, for the considered energy range, we ignored this energy dependence because of its negligible effects on the results.

We use the same nuclear matter densities employed to derive the DFC potential in order to calculate the M3Y one. The two potentials are shown in Fig. 3. We notice that although the two potentials are built on two different interactions ( $V_{\alpha\alpha}$  and  $v_{nn}$ , which are separately parametrized) they are almost indistinguishable. At the center ( $R=0$ ),  $V_{M3Y}/V_{DFC}=1.036$ . This may indicate that the DFC potential is as realistic as the M3Y one.

From Table I we notice, also, that the two deep and shallow sets, *A* and *B*, respectively, of the imaginary part of the optical potential yielded similar elastic scattering results. This means that the calculations are insensitive to the strength  $W_0$  used in the fit of experimental data. This indi-

cates, as mentioned in Ref. [11], that the absorption takes place on the same region of the nuclear surface independently of the strength  $W_0$ . We notice, further, that the fitting is insensitive to the imaginary potential at the strong absorption radius [1]  $R_{sa}=9.7$  fm.

The volume integral per interacting nucleon pair of the real DFC potential  $J_R$  has the same energy dependence as  $N$ , where  $J_R = -413.5N$  MeV fm<sup>3</sup> [8]. The obtained values of the volume integral of the imaginary WS potential  $J_I$  are listed in Table I. There is a linear energy dependence similar to that observed for the M3Y DF potential analysis [11] as shown in the middle part of Fig. 2. At the same time, we notice that  $J_I$  has the same energy dependence factor  $\sim(1 - 0.005E)$  as  $N$ . However, values of  $J_I$  obtained from set *B* do not show any clear energy correlation.

The energy dependence of the total reaction cross section  $\sigma_R$  obtained from the present analysis is shown in the upper part of Fig. 2 in comparison with that of Ref. [11]. As clearly noticed, both results are identical and have a linear energy dependence. It is clear that at near-barrier energies the total reaction cross section is very small because it takes place at the nuclear surface in a very narrow domain. This domain broadens with increasing energy and consequently  $\sigma_R$  increases.

Finally, from the present analysis, we can extract two interesting conclusions. First, the DFC potential renormalized by a real energy-dependent factor has successfully reproduced the elastic scattering differential cross section data for HI reactions at near- and sub-barrier energies. The success of the DFC potential to predict the data is on the same foot with that of the M3Y one. Second, the DFC and M3Y DF potentials based upon the same nuclear matter densities are identical all over the radius range 0–15 fm.

- 
- [1] M. El-Azab Farid and M.A. Hassanain, Nucl. Phys. **A678**, 39 (2000), and references therein.  
 [2] M. El-Azab Farid and M.A. Hassanain, Nucl. Phys. **A697**, 183 (2001).  
 [3] M. El-Azab Farid and M.A. Hassanain, Phys. Rev. C (to be published).  
 [4] G.R. Satchler and W.G. Love, Phys. Rep. **55**, 183 (1979).  
 [5] B. Buck, C.B. Dover, and J.P. Vary, Phys. Rev. C **11**, 1803 (1975).  
 [6] Y. Goto and H. Horiuchi, Prog. Theor. Phys. **62**, 662 (1979).  
 [7] M. El-Azab Farid, J. Phys. G **16**, 461 (1990).

- [8] M. El-Azab Farid, Z.M.M. Mahmoud, and G.S. Hassan, Phys. Rev. C **64**, 014310 (2001), and references therein.  
 [9] M. El-Azab Farid, Z.M.M. Mahmoud, and G. S. Hassan, Nucl. Phys. **A691**, 671 (2001).  
 [10] M. El-Azab Farid, Phys. Rev. C (to be published).  
 [11] J.C. Pacheco, B. Bilwes, F. Sanchez, J.A. Ruiz, J. Diaz, J.L. Ferrero, and D. Kadi-Hanifi, Nucl. Phys. **A588**, 537 (1995).  
 [12] O.M. Knyazov and E.F. Hefter, Z. Phys. A **301**, 277 (1981).  
 [13] R.D. Woods and D.S. Saxon, Phys. Rev. **95**, 577 (1954).  
 [14] N.M. Clarke (unpublished).